Sonic Boom Adjoint Methodology and its Applications

Sriram K. Rallabhandi*

National Institute of Aerospace, Hampton, VA 23666

This paper presents an approach to predict the sensitivity of the sonic boom ground signatures by numerically solving the augmented Burgers' equation along with its discrete adjoint. The discrete adjoint equations are derived and solved. The exactness of the adjoint sensitivities is verified against derivatives obtained using the complex variable approach. Under- and off-track ground signature sensitivities to different design variables may be obtained efficiently. The formulation of the coupling between boom adjoint and CFD adjoint is derived and discussed. This formulation represents the first time in literature that boom propagation and CFD are formally coupled for the purpose of obtaining gradients of a ground based objective with respect to the aircraft shape design variables. The coupled formulation is effective in calculating discretely accurate sensitivities, and should be an extremely useful tool in the design of supersonic cruise low-boom aircraft.

Nomenclature

c_0	Ambient speed of sound, m/s.
C_ν	Dimensionless dispersion.
D	Vector of design variables.
G	Ray tube area, m^2.
k_n	Scaling factor due to ray-tube speading and stratification.
L	Lagrangian.
l_n	Objective/cost function for adjoint calculation.
m_ν	Dispersion parameter.
N	Number of steps during propagation.
P	Dimensionless pressure.
p	Pressure waveform during propagation.
p_{ref}	Reference pressure.
p_t	Target ground signature.
q, r, t	Intermediate pressure waveforms.
$t^{'}$	Retarded time.
$\overline{x}$	Shock formation distance of a plane wave.
α_0^{tv}	Thermo-viscous attenuation coefficient.
A^n, B^n	Matrices during the first relaxation process.

*Senior Research Engineer, National Institute of Aerospace.

A_2^n, B_2^n	Matrices during the second relaxation process.
A_3^n, B_3^n	Matrices during absorption process.
β	$1 + \frac{\gamma-1}{2}$.
δ	Diffusion parameter.
Γ	Dimensionless thermo-viscous parameter.
γ	Ratio of specific heats, 1.4.
$\lambda_n, \beta_n, \gamma_{0,n}, \gamma_{1,n}$	Adjoint vectors.
ω_0	Angular frequency.
ρ_0	Ambient density.
σ	Non-dimensional distance.
τ	Dimensionless time.
τ_ν	Dimensionless time for each relaxation mode.
τ'	Intermediate retarded time coordinate.
θ_ν	Dimensionless relaxation time parameter.

I. Introduction and Motivation

Meeting the stringent noise and design constraints for an efficient supersonic aircraft is an extremely challenging problem. Aircraft designers are actively looking for ways to modify their concepts to meet the goals associated with efficient supersonic flight. One of the primary ways to achieve improved sonic boom footprint is through aircraft shaping. The Shaped Sonic Boom Demonstrator (SSBD)[1] program verified, via flight testing, that aircraft shaping is an effective strategy for changing the boom signature on the ground. Therefore, the main objective in supersonic aircraft design exercises is to obtain an aircraft concept and shape that will produce a desirable ground signature. Computational Fluid Dynamics (CFD) shape optimization using adjoint sensitivities is a promising approach, where a desired off-body pressure distribution is achieved by using the sensitivity of the off-body pressure profiles to the aircraft shape design variables. However, near-field targets used in the adjoint CFD shape optimization exercises are generally based on experience, not on the sensitivity to a desired ground signature. Furthermore, near-field targets or desired off-body pressures are just intermediate waveforms during propagation; the loudness and noise metrics are based on the ground signatures. Therefore, there is a need for a methodology that takes the desired ground signatures as input, and generates appropriate near-field waveforms that can be used in shape optimization studies.

This paper proposes an adjoint methodology based on augmented Burgers' equation to help the designer generate near-field waveforms based on desired ground signatures. The desired ground signatures could be modifications of the baseline ground signature; for example removing some high frequency content (shocks) or signatures based on experience or signatures that have extremely low perceived loudness such as variations of a sine wave. The adjoint method allows the computation of the sensitivity of the ground signature to the initial near-field pressure waveform. A gradient-based optimization procedure may be used to move the baseline near-field distribution to a new distribution so that the desired ground signature can be obtained. Computing the sensitivity of the ground signature to the near-field waveforms can be extremely useful in tailoring the near-field pressure waveform to yield the desired ground signatures. In addition, by coupling the sonic boom adjoint methodology to an adjoint CFD solver, the sensitivity of the ground based boom metric with respect to the aircraft shape design variables can be obtained efficiently. In this study, coupling with FUN3D[2] was accomplished and large-scale demonstrations have also been performed. This coupling allows aircraft shape optimization directly using sonic boom target ground signatures.

The main goals of this paper are:

- To formulate the boom adjoint problem
- Predict the sensitivities of the ground signature w.r.t. selected design variables

- Demonstrate the use of adjoint sensitivities to achieve a near-field that produces the desired ground signature
- Couple the boom adjoint method with an adjoint CFD solver and demonstrate that aircraft shape optimization can be performed.

II. Mathematics of Boom Adjoint

This section presents the mathematics behind the boom adjoint methodology. The primal problem refers to the augmented Burgers' propagation.[3] The augmented Burgers' equation is given in Equation 1.

$$\frac{\partial P}{\partial \sigma} = P\frac{\partial P}{\partial \tau} + \frac{1}{\Gamma}\frac{\partial^2 P}{\partial \tau^2} + \Sigma_\nu \frac{C_\nu \frac{\partial^2}{\partial \tau^2}}{1+\theta_\nu \frac{\partial}{\partial \tau}} P - \frac{1}{2G}\frac{\partial G}{\partial \sigma}P + \frac{1}{2\rho_0 c_0}\frac{\partial(\rho_0 c_0)}{\partial \sigma}P \tag{1}$$

An operator splitting scheme[4] is used to solve a set of five equations under the assumption that if the time step is small, the error induced by splitting is small. The following set of equations are solved during boom propagation.

$$\begin{aligned}
\frac{\partial P}{\partial \sigma} &= p\frac{\partial P}{\partial \tau}\text{[Non-Linearity]} \\
\frac{\partial P}{\partial \sigma} &= \frac{1}{\Gamma}\frac{\partial^2 P}{\partial \tau^2}\text{[Absorption]} \\
\frac{\partial P}{\partial \sigma} &= \Sigma_\nu \frac{C_\nu \frac{\partial^2}{\partial \tau^2}}{1+\theta_\nu \frac{\partial}{\partial \tau}} P\text{[Molecular Relaxation]} \\
\frac{\partial P}{\partial \sigma} &= -\frac{1}{2G}\frac{\partial G}{\partial \sigma}P\text{[Ray Tube Spreading]} \\
\frac{\partial P}{\partial \sigma} &= \frac{1}{2\rho_0 c_0}\frac{\partial(\rho_0 c_0)}{\partial \sigma}P\text{[Atmospheric Stratification]}
\end{aligned} \tag{2}$$

In these equations, $P\ (\sigma,\tau) = \frac{p}{p_{ref}}$, where p_{ref} is a reference pressure. The non-dimensional distance is given by $\sigma = \frac{x}{\overline{x}}$, where $\overline{x} = \frac{\rho_0 c_0^3}{\beta \omega_0 p_{ref}}$ is the shock formation distance of a plane wave with peak pressure p_{ref}. The dimensionless time τ is defined as $\tau = \omega_0\ t'$. The dimensionless thermo-viscous parameter is defined as $\Gamma = \frac{1}{\alpha_0^{tv}\overline{x}}$, where the thermo-viscous attenuation coefficient is given by: $\alpha_0^{tv} = \frac{\delta \omega_0^2}{2c_0^3}$. The dimensionless relaxation time parameter is given by $\theta_\nu = \omega_0 t_\nu$. The dimensionless dispersion parameter is given by $C_\nu = \frac{m_\nu \tau_\nu \omega_0^2}{2c_0}\overline{x}$, where m_ν is a function of the equilibrium and frozen sound speeds in a particular medium.

The relaxation term can be simplified into Equation 3. Discretization schemes are different for different propagation phenomena. For the relaxation terms, the pressure is advanced in time using a Crank-Nicholson scheme for the diffusion term and central differencing scheme for the mixed derivative term. Equation 4 represents the effect of first relaxation and scaling due to ray tube area (G) spreading and stratification. The matrices included in these equations are provided in the Appendix. Based on the discretization scheme used, the matrices are tridiagonal; hence Thomas algorithm[5] may be used to solve the system efficiently. Since there are two relaxation phenomena corresponding to Oxygen and Nitrogen, Equations 4 and 5 are each solved using their respective values for C_ν and θ_ν.

$$\frac{\partial p}{\partial \sigma} = C_\nu \frac{\partial^2 p}{\partial \tau^2} - \theta_\nu \frac{\partial^2 p}{\partial \tau \partial \sigma} \tag{3}$$

$$A^n q_n = k_n B^n p_{n-1} \tag{4}$$

$$A_2^n r_n = B_2^n q_n \tag{5}$$

For the absorption equation, a Crank-Nicholson scheme is used for advancing the pressure in time. Using this discretization scheme, the absorption phenomenon also transforms into a tridiagonal matrix problem as given in Equation 6, which may be solved to obtain t_n.

$$A_3^n t_n = B_3^n r_n \tag{6}$$

The non-linear equation is solved using the Poisson solution and is dependent on the solution from the absorption equation as given in Equation 7. In this equation, t_n is a function with two arguments, propagation distance (σ_n) and the time coordinate; t_n can be thought of as a matrix such that $t_{n,i}$ represents the σ_n^{th} row and τ_i^{th} column. This retarded time equation is solved via re-interpolation as shown in Equation 8, where τ' is the retarded coordinate given by $\tau'_{n,i} = \tau_i - t_{n,i}\Delta\sigma_n$, $\Delta\sigma_n = \sigma_n - \sigma_{n-1}$, and j is an index such that $\tau'_{n,i-1} < \tau_j < \tau'_{n,i}$. Expanding the terms results in the discretized equation for the non-linear part of the Burgers' equation primal problem as given in Equation 9.

$$p(\sigma_n, \tau_i) = t_n(\sigma_n, \tau_i + t_{n,i}\Delta\sigma_n) \tag{7}$$

$$p_{n,j} = t_{n,i-1} + \frac{t_{n,i} - t_{n,i-1}}{\tau'_{n,i} - \tau'_{n,i-1}} \left(\tau_j - \tau'_{n,i-1}\right) \tag{8}$$

$$p_{n,j} = t_{n,i-1} + \frac{t_{n,i} - t_{n,i-1}}{\Delta\tau - (t_{n,i} - t_{n,i-1})\Delta\sigma_n} \left[\tau_j - \tau_{i-1} + t_{n,i-1}\Delta\sigma_n\right] = f_{n,j} \tag{9}$$

The ray tube spreading and atmospheric stratification are simply scaling terms - these are included in the k factor in Equation 4. For the solution of the augmented Burgers' equation, Equations 4, 5, 6 and 9 are solved repeatedly, in that order, for $n = 1 \ldots N$ time steps and at each stage the pressure is updated, while also successively updating intermediate values: r, q, and t.

Adjoint

The discrete adjoint equations are derived in this section based on a similar implementation given by Nielsen et.al.[6] A Lagrangian is first written to account for the complete propagation process. Suppose D is the vector of design variables and l_n is the objective function. Then the Lagrangian corresponding to this objective may be written as in Equation 10. Taking the derivative of the Lagrangian with respect to D results in Equation 11, where it has been assumed that the objective does not depend explicitly on the intermediate pressure vectors r, q, and t. Furthermore, the matrices themselves do not vary with the initial pressure profile, which is the design variable vector chosen in this study. If the design variables are different, this equation needs to be modified accordingly to construct the discrete adjoint equations.

$$\begin{aligned} L(p,q,r,t,D) = &\sum_{n=1}^{N} l_n(p,D)\Delta\sigma_n + \sum_{n=2}^{N} \gamma_{0,n}^T \left[A^n q_n - k_n B^n p_{n-1}\right]\Delta\sigma_n + \sum_{n=1}^{N} \gamma_{1,n}^T \left[A_2^n r_n - B^n q_n\right]\Delta\sigma_n \\ &+ \sum_{n=1}^{N} \beta_n^T \left[A_3^n t_n - B_3^n r_n\right]\Delta\sigma_n + \sum_{n=1}^{N} \lambda_n^T \left[p_n - f^n(t_n, D)\right]\Delta\sigma_n + \gamma_{0,1}^T \left[A^1 q_1 - k_1 B^1 D\right]\Delta\sigma_n \end{aligned} \tag{10}$$

$$\begin{aligned} \frac{dL}{dD} = &\sum_{n=1}^{N} \left[\frac{\partial l_n}{\partial D} + \frac{\partial l_n}{\partial p_n}\frac{\partial p_n}{\partial D}\right]\Delta\sigma_n + \sum_{n=2}^{N} \gamma_{0,n}^T \left[A^n \frac{\partial q_n}{\partial D} - k_n B^n \frac{\partial p_{n-1}}{\partial D}\right]\Delta\sigma_n \\ &+ \sum_{n=1}^{N} \gamma_{1,n}^T \left[A_2^n \frac{\partial r_n}{\partial D} - B_2^n \frac{\partial q_n}{\partial D}\right]\Delta\sigma_n + \sum_{n=1}^{N} \beta_n^T \left[A_3^n \frac{\partial t_n}{\partial D} - B_3^n \frac{\partial r_n}{\partial D}\right]\Delta\sigma_n \\ &+ \sum_{n=1}^{N} \lambda_n^T \left[\frac{\partial p_n}{\partial D} - \frac{\partial f_j^n}{\partial t_n}\frac{\partial t_n}{\partial D}\right]\Delta\sigma_n + \gamma_{0,1}^T \left[A^1 \frac{\partial q_1}{\partial D} - k^1 B^1\right]\Delta\sigma_n \end{aligned} \tag{11}$$

Collecting the $\frac{\partial p_n}{\partial D}$, $\frac{\partial t_n}{\partial D}$, $\frac{\partial r_n}{\partial D}$ and $\frac{\partial q_n}{\partial D}$ terms from Equation 11 and equating them to zero results in four adjoint equations that are solved iteratively backwards in time. Collecting all the $\frac{\partial p_n}{\partial D}$ terms, and simplifying yields Equation 12. Similarly, collecting the $\frac{\partial t_n}{\partial D}$, $\frac{\partial r_n}{\partial D}$, and $\frac{\partial q_n}{\partial D}$ terms, we have Equations 13, 14 and 15 respectively. The adjoint solution process involves solving Equations 12, 13, 14, and 15 iteratively. Equation 12 is solved initially by assuming $\gamma_{0,N+1} = 0$ since there are no "N+1" terms in our primal propagation problem. The intermediate adjoints are successively updated and solved. The primal problem is solved first, and relevant pressure vectors are stored for use in the adjoint process.

$$\lambda_n^T = -\frac{\partial l_n}{\partial p_n} + \gamma_{0,n+1}^T k_{n+1} B^{n+1} \tag{12}$$

$$\beta_n^T A_3^n = \lambda_n^T \frac{\partial f_j^n}{\partial t_n} \tag{13}$$

$$\gamma_{1,n}^T A_2^n = \beta_n^T B_3^n \tag{14}$$

$$\gamma_{0,n}^T A^n = \gamma_{1,n}^T B_2^n \tag{15}$$

In most boom design studies, the objective is to achieve a desired target signature. With this in mind, the cost function chosen in this study is given in Equation 16. The objective is dependent only on the final (ground) pressure distribution i.e. $l_n = 0 \; \forall \; n < N$. The analytical derivative of the cost function (Equation 17) can be used in Equation 12 to start the adjoint calculation process.

$$l_N = \frac{1}{2} \sum_{i=1}^{M} \left[p_N^i - p_t^i \right]^2 d\tau \tag{16}$$

$$\frac{\partial l_N}{\partial p_N^i} = \left[p_N^i - p_t^i \right] d\tau \tag{17}$$

Equation 9 may be differentiated to obtain the partial derivative terms needed in the adjoint calculation. Based on the definition of τ', the non-linear residual in Equation 9 may be expanded as Equation 18. Taking the partial derivatives with respect to t_i^n and t_{i-1}^n yields Equations 19 and 20 respectively. These are used to populate the Jacobian matrix in Equation 13.

$$f_j^n(t^n) = t_{i-1}^n + \frac{t_i^n - t_{i-1}^n}{\Delta\tau - (t_i^n - t_{i-1}^n)\Delta\sigma_n} \left[\tau_j - \tau_{i-1} + t_{i-1}^n \Delta\sigma_n \right] \tag{18}$$

$$\frac{\partial f_j^n}{\partial t_{i-1}^n} = 1 - \frac{\Delta\tau \left[\tau_j - \tau_{i-1} + t_{i-1}^n \Delta\sigma_n \right]}{\left[\Delta\tau - (t_i^n - t_{i-1}^n)\Delta\sigma_n \right]^2} + \frac{(t_i^n - t_{i-1}^n)\Delta\sigma_n}{\left[\Delta\tau - (t_i^n - t_{i-1}^n)\Delta\sigma_n \right]} \tag{19}$$

$$\frac{\partial f_j^n}{\partial t_i^n} = \frac{\Delta\tau \left[\tau_j - \tau_{i-1} + t_{i-1}^n \Delta\sigma_n \right]}{\left[\Delta\tau - (t_i^n - t_{i-1}^n)\Delta\sigma_n \right]^2} \tag{20}$$

Gradient Calculation

For adjoint solutions satisfying Equations 12-15, the only remaining term is the last term shown in Equation 21. After the adjoint equations are solved, the last solution of Equation 15 is multiplied with the scalar factor and the tridiagonal matrix of the first relaxation process to generate the gradient values needed for optimization.

$$\frac{dL}{dD} = -\gamma_{0,1}^T k_1 B^1 \Delta\sigma_1 \tag{21}$$

III. Implementation and Verification

Implementation of the boom propagation as well as the adjoint process begins by obtaining a CFD near-field pressure distribution. The propagation process first discretizes this original input waveform into a desired uniform spacing grid. This transformation or mapping of the CFD near-field to input for boom propagation is accomplished through linear interpolation followed by zero-padding on both ends. Therefore, if the initial near-field is represented by p_0, the intermediate near-field, p_0^I, is given in Equation 22, where ps is a scaling factor to account for the conversion to a non-dimensional form used within the propagation process. These waveforms are plotted in Figures 1(a) and 1(b) respectively. In the previous section, where sonic boom adjoint methodology and gradient calculation of a cost function are derived, the design vector D is actually p_0^I.

From the adjoint methodology, the gradient $\frac{dL}{dp_0^I}$ is calculated. In order to obtain modifications to the near-field waveform, the derivative $\frac{dL}{dp_0}$ is needed. From chain rule differentiation, $\frac{dL}{dp_0} = \frac{dL}{dp_0^I} \frac{dp_0^I}{dp_0}$. Using Equations 23 and 24, the Jacobian matrix $\frac{dp_0^I}{dp_0}$ can be populated and multiplied with the gradients from

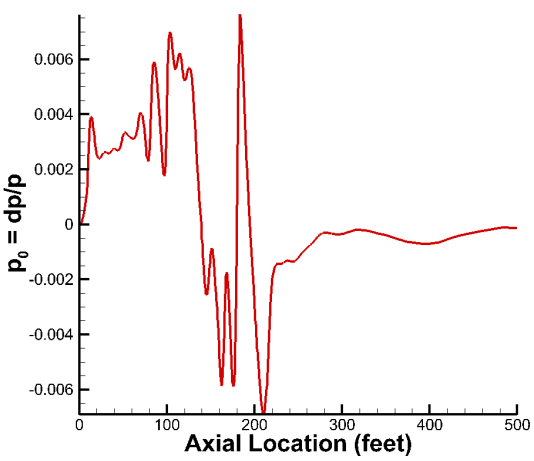

(a) Original near-field pressure distribution

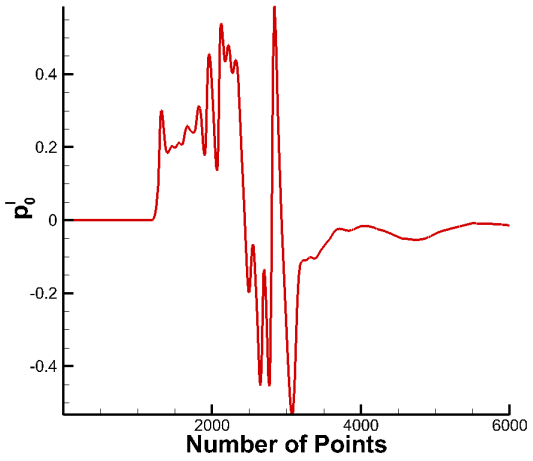

(b) Intermediate near-field pressure distribution

Figure 1. Near-field pressure waveforms for verification of adjoint

the adjoint process to generate the derivatives needed to perform near-field waveform modification for minimizing a chosen objective or cost function.

$$p^I_{0,i} = ps\left[p_{0,ii} + \frac{p_{0,ii+1} - p_{0,ii}}{X_{0,ii+1} - X_{0,ii}}(X^I_{0,i} - X_{0,ii})\right] \tag{22}$$

$$\frac{dp^I_{0,i}}{dp_{0,ii}} = ps\left[1 - \frac{X^I_{0,i} - X_{0,ii}}{X_{0,ii+1} - X_{0,ii}}\right] \tag{23}$$

$$\frac{dp^I_{0,i}}{dp_{0,ii+1}} = ps\frac{X^I_{0,i} - X_{0,ii}}{X_{0,ii+1} - X_{0,ii}} \tag{24}$$

A ground signature can be obtained by using the propagation process. A target ground signature may then be used to generate a cost function that drives the adjoint process. A sample, arbitrary target signature along with the original signature is plotted in Figure 2. The target signature deviates significantly from the original signature for most of the mid-expansion region; the shock in this region is completely removed in the desired target.

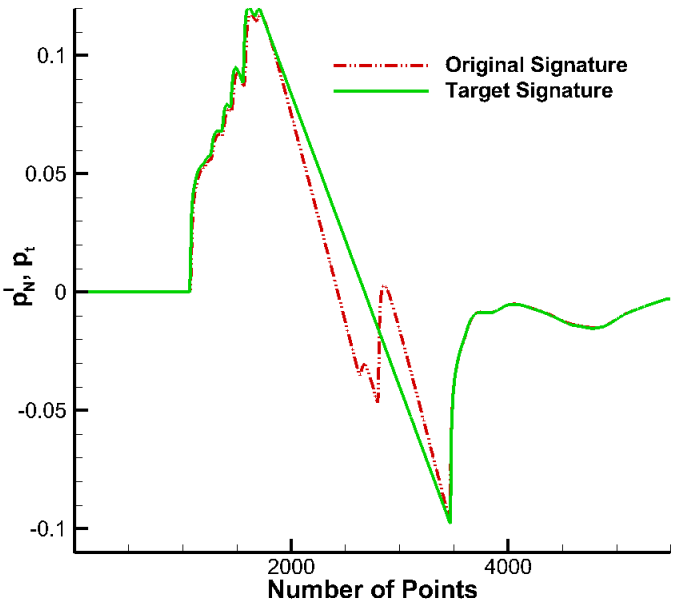

Figure 2. Ground Signature and Target

The adjoint method is run using the cost function described in Equation 16. To verify the accuracy of the adjoint implementation, comparisons are made with gradients generated through the use of a complex

variables approach,[7,8] which has been applied in several other adjoint gradient verifications. According to the complex variable derivative approach, the first derivative of a real-valued function $f(x)$, given by Equation 25, is obtained by expanding the function in a complex-valued Taylor series using an imaginary perturbation $i\epsilon$. The main advantage of the complex variable method is that true second-order accuracy is achieved by selecting step sizes without incurring subtractive cancellation errors typically present in real-valued finite differences. The propagation process is modified to work with complex variables and the derivatives are calculated. For all the results shown in this study, the imaginary step size was chosen to be 10^{-20}. Table 1 compares the adjoint gradients $\frac{dL}{dp_0^I}$ against the complex variable gradients for some arbitrary grid point locations. It is seen that the results using adjoint implementation exhibit excellent agreement with the complex-variable approach, differing at most in the tenth digit. This verifies that the gradients obtained using the adjoint approach are correct to at least ten digits of numerical precision.

$$\frac{\partial f}{\partial x} = \frac{Im\left[f(x+i\epsilon)\right]}{\epsilon} + O(\epsilon^2) \tag{25}$$

Table 1. Comparison of the Adjoint and Complex Variable Gradients

Grid Point	Adjoint Gradient	Complex Variable Gradient
1200	0.00000019721521	0.00000019721423
2000	-0.00000060412713	-0.00000060411918
2576	-0.00000473528829	-0.00000473528673
4012	-0.00000000193716	-0.00000000193713
5001	0.00000000932531	0.00000000932531
6739	-0.00000000021543	-0.00000000021544
8547	-0.00000000000185	-0.00000000000186

The gradient of the cost function with respect to p_0^I is depicted in Figure 3. The plot is truncated around grid point 3000 because beyond this point the gradient values are very close to zero and the plot remains a flat line. It is seen that the gradients are quite noisy near the front portion of the waveforms. The same pattern is observed in the complex gradients. The adjoint gradients are multiplied with the interpolation Jacobians in Equations 23, 24, and the sensitivity of the cost function to the original CFD near-field is obtained. This is depicted in Figure 4, where the gradient is super-imposed with the original CFD near-field pressure waveform. In contrast to the intermediate gradient from Figure 3, the gradient with respect to the CFD near-field does not exhibit oscillatory behavior, which is the result of linear interpolation. The gradient $\frac{dL}{dp_0}$ can be used to minimize the cost function by changing the CFD near-field distribution using a gradient-based optimization scheme.

IV. Coupled CFD/Boom Adjoint Formulation

To enable formal design of complex aerospace configurations, the boom-adjoint formulation is coupled with the NASA Langley unstructured CFD solver FUN3D.[2] The FUN3D software solves the compressible and incompressible forms of the steady and unsteady Euler and Reynolds-averaged Navier-Stokes equations on general static and dynamic mixed-element grid discretizations, which may optionally include overset grid topologies. The software has been used for a broad class of aerodynamic analysis and design simulations across the speed range. FUN3D also offers a discretely-consistent adjoint implementation that has been used to perform mathematically-rigorous design optimization, error estimation, and formal mesh adaptation for complex geometries and flow-fields in massively parallel computing environments.[6,9] These applications include accurate analysis and design optimization of aircraft concepts aimed at sonic boom mitigation.[10,11] Such simulations have traditionally relied on objective functions posed in the near-field within 20 body lengths of the vehicle, ultimately yielding an indirect approach which fails to formally address the pressure signature on the ground. However, the adjoint approach for the propagation methodology developed here offers an exciting opportunity to formally couple existing near-field CFD analysis and design capabilities with the methodology used to predict pressure signatures at the ground. Finally, it should be noted that FUN3D also offers a discretely-consistent forward mode of differentiation. A scripting procedure[12] can be used to automatically convert the baseline source code to a complex-variable formulation as described above. In this manner, sensitivities of all FUN3D outputs with respect to any input parameter may be easily evaluated.

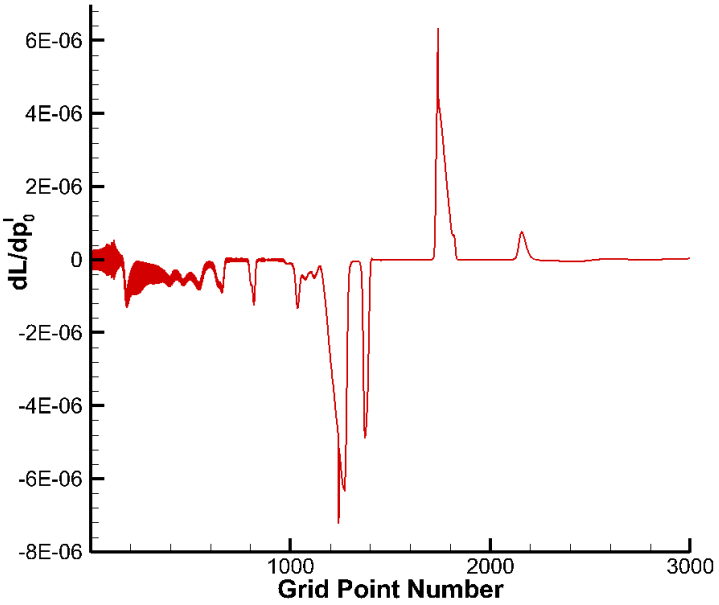

Figure 3. Intermediate gradient $\frac{dL}{dp_0^I}$

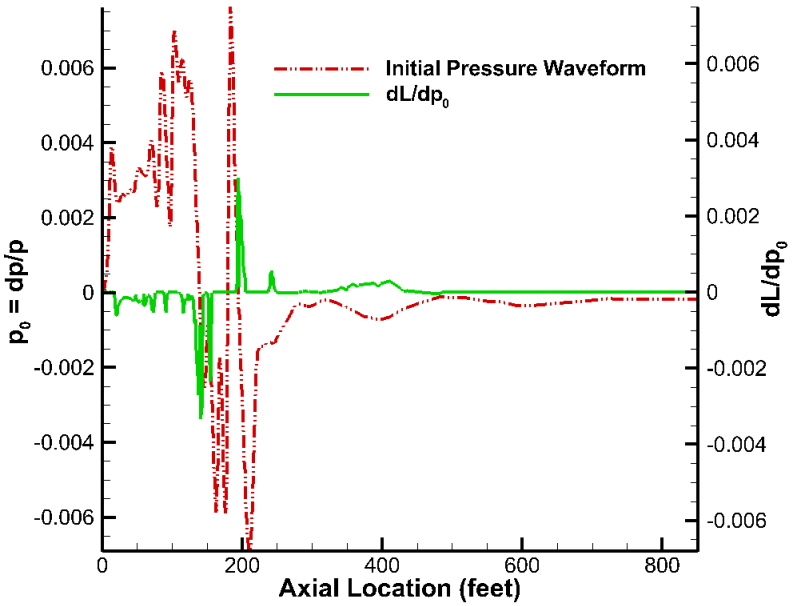

Figure 4. Gradient $\frac{dL}{dp_0}$ along with p_0

The coupled formulation is described from the perspective of the CFD solver. In this approach, the interface between FUN3D and boom propagation takes the form of a one-dimensional pressure distribution p_0 evaluated at a fixed distance from the aircraft in the near-field CFD mesh. The CFD solution determined on the unstructured mesh is used to construct this pressure distribution, which serves as the input for the boom analysis problem. Given p_0, the forward mode of boom analysis evaluates the cost function l_N. The adjoint mode then determines the sensitivity of the cost function to p_0, which is a horizontal vector denoted dl_N/dp_0.

The relationship between the near-field pressure signature and the CFD solution is described as

$$p_0 = \mathbf{T}(\mathbf{Q}, \mathbf{X}), \tag{26}$$

where the vectors $\mathbf{Q}$ and $\mathbf{X}$ represent the CFD solution and mesh, respectively; and $\mathbf{T}$ is a transformation mapping the CFD solution to the desired pressure distribution p_0. The Lagrangian for the coupled formulation is defined as

$$\mathbf{L}\left(\mathbf{D}, \mathbf{Q}, \mathbf{X}, \mathbf{\Lambda}_f, \mathbf{\Lambda}_g, \mathbf{\Lambda}_b\right) = l_N + \left[\mathbf{\Lambda}_g\right]^T \mathbf{G} + \left[\mathbf{\Lambda}_f\right]^T \mathbf{R} + \left[\mathbf{\Lambda}_b\right]^T \left(p_0 - \mathbf{T}\right). \tag{27}$$

Here, $\mathbf{\Lambda}_f$ and $\mathbf{\Lambda}_g$ are adjoint variables corresponding to the discrete flow equations $\mathbf{R}(\mathbf{Q}, \mathbf{X}, \mathbf{D}) = 0$ and grid equations $\mathbf{G}(\mathbf{X}, \mathbf{D}) = 0$, respectively; $\mathbf{\Lambda}_b$ is a vector of adjoint variables associated with the boom interface given by Equation 26; and $\mathbf{D}$ is a vector of design variables. In the current study, the design variables consist of geometric parameters defining the discrete surface grid for the aircraft.

Differentiating the Lagrangian with respect to $\mathbf{D}$ and equating the coefficients of $\partial p_0/\partial \mathbf{D}$, $\partial \mathbf{X}/\partial \mathbf{D}$, and $\partial \mathbf{Q}/\partial \mathbf{D}$ to zero yields the following system of adjoint equations:

$$\begin{aligned} &\left[\tfrac{dl_N}{dp_0}\right]^T + \mathbf{\Lambda}_b = 0, \\ &\left[\tfrac{\partial \mathbf{R}}{\partial \mathbf{Q}}\right]^T \mathbf{\Lambda}_f - \left[\tfrac{\partial \mathbf{T}}{\partial \mathbf{Q}}\right]^T \mathbf{\Lambda}_b = 0, \\ &\left[\tfrac{\partial \mathbf{G}}{\partial \mathbf{X}}\right]^T \mathbf{\Lambda}_g + \left[\tfrac{\partial \mathbf{R}}{\partial \mathbf{X}}\right]^T \mathbf{\Lambda}_f - \left[\tfrac{\partial \mathbf{T}}{\partial \mathbf{X}}\right]^T \mathbf{\Lambda}_b = 0. \end{aligned} \tag{28}$$

Recall that the vector dl_N/dp_0 is computed using the adjoint mode of boom analysis as described in Sections II and III. Assuming that the adjoint variables satisfy Equations 28 and that the transformation $\mathbf{T}$ given by Equation 26 does not explicitly depend on $\mathbf{D}$, the desired sensitivity derivatives of the ground signature with respect to the aircraft geometry are then calculated as follows:

$$\frac{\partial \mathbf{L}}{\partial \mathbf{D}} = \left[\mathbf{\Lambda}_g\right]^T \frac{\partial \mathbf{G}}{\partial \mathbf{D}} + \left[\mathbf{\Lambda}_f\right]^T \frac{\partial \mathbf{R}}{\partial \mathbf{D}}. \tag{29}$$

Note that the computational cost associated with the solution of Equations 28 is similar to that of their traditional forward-mode counterparts, and the cost required to evaluate Equation 29 is trivial. In this manner, the approach outlined here ultimately enables a discretely consistent sensitivity analysis to be performed for the coupled system at the cost of a single forward-mode analysis, even for very large numbers of design variables.

V. Applications

This section presents a couple of applications using the boom adjoint methodology developed in this study. Figure 5 depicts the ground signature corresponding to a sample off-body pressure distribution along with a desired target signature. The target signature varies from the original signature only in a small region of the mid-body expansion. The adjoint method is used to compute the sensitivity of the objective with respect to the near-field pressure distribution. A steepest descent method is used to drive the optimizer to achieve a modified near-field pressure waveform that will result in the desired ground signature.

The optimizer was run for 2200 iterations; each iteration requires approximately 5 seconds on a 64-bit Intel Dual Core 2.8 GHz processor with 3GB RAM. When the first case was run, the optimizer's progress was extremely slow. The total number of design variables is equal to the number of discrete points in the original near-field pressure distribution (471 in this case). Out of these, because the target differs from the ground signature in a limited region, only a few of them are active, while a majority of the design variables are inactive. This forces the step-size to be small, in turn causing the convergence to be slow. In order to improve convergence behavior, the number of active variables is decreased to only consider the relevant ones. Therefore, only the near-field waveform within the boxed region in Figure 6 is allowed to vary based on the adjoint sensitivity information. The other locations are constrained to be the same as the original near-field waveform. The adjoint calculation and gradient-based optimization

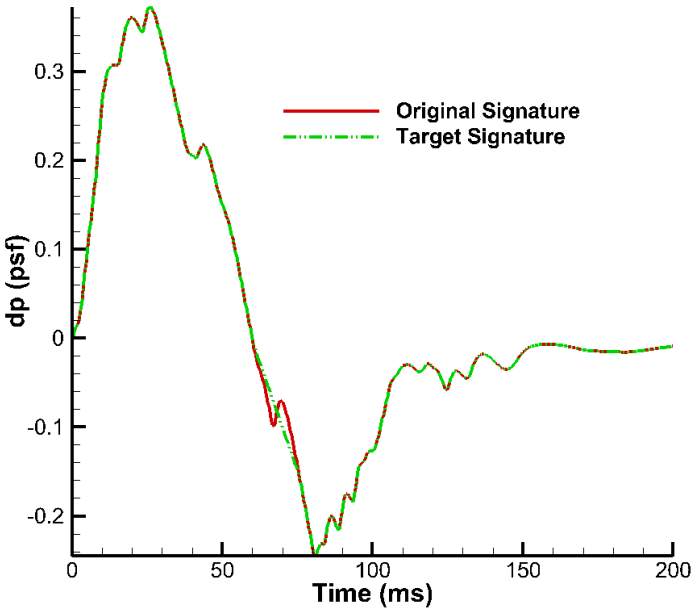

Figure 5. Ground signature and target comparison

process is run. Figures 6 and 7 show the near-field waveforms and the ground signatures as the iteration number increases. A significant improvement is seen within the first 100 iterations; after about 2200 iterations the ground signature almost reaches the desired target ground signature. Observation of the near-field waveforms in Figure 6 shows that to achieve the target signature on the ground, additional small shocks and expansions are needed in the off-body pressure profile. Based on the propagation process, the interplay of these shocks and expansions results in the desired target on the ground.

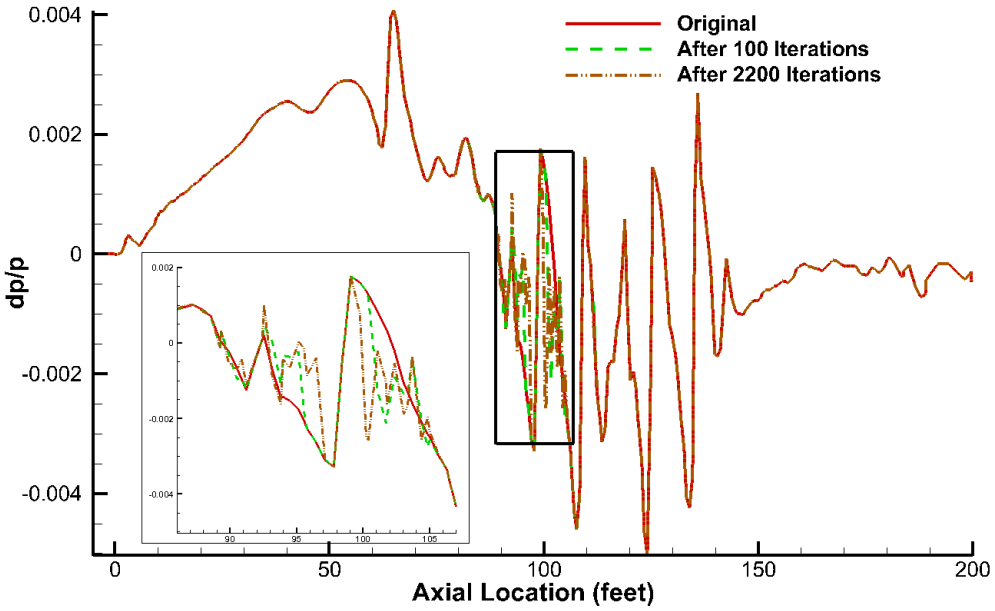

Figure 6. Near-field pressure waveform comparison with limited active variables

Figure 8 compares the convergence behavior of the two cases. It is evident that keeping only the relevant design variables active significantly improves the convergence behavior of the problem.

A. CFD coupled Implementation

To evaluate the ability of the coupled formulation to design a configuration of interest, a near-field grid for the aircraft geometry shown in Figure 9 has been generated using the procedures described elsewhere[13,14] and is shown in Figure 10. This grid generation approach is a heuristic technique to

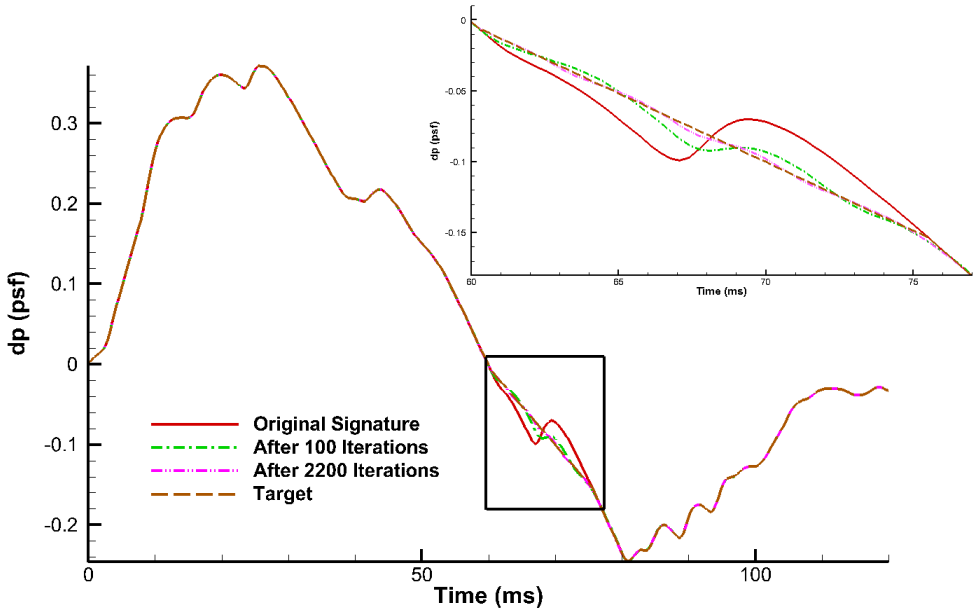

Figure 7. Ground signature comparison with limited active variables

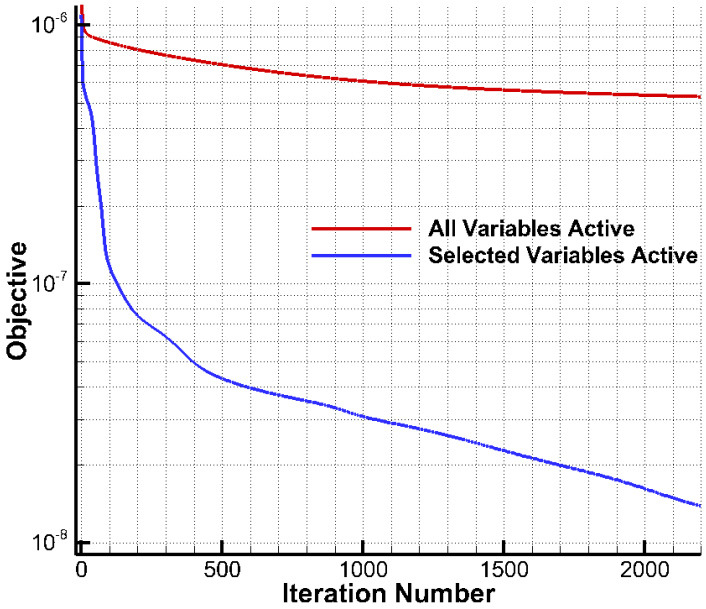

Figure 8. Iteration history comparison

align the mesh topology a priori with the expected primary off-body shock structures. A more rigorous adjoint-based approach to mesh adaptation for such problems is described in literature;[11] however, the manual approach used here is sufficient for the current test. The CFD grid utilizes a plane of symmetry along the centerline and contains 4,197,284 nodes and 24,371,026 tetrahedral elements. The surface mesh for the aircraft has been parameterized using the packages MASSOUD[15] and BANDAIDS.[16] These methodologies are based on free-form deformation techniques which provide a compact set of design variables describing changes to a discrete surface mesh. Both approaches provide the analytic sensitivities required by the discrete adjoint formulation of the near-field CFD problem. MASSOUD[15] is designed for use with common aircraft-centric geometries and provides a set of intuitive design variables such as thickness, camber, twist, shear, and planform parameters. For the current test, this approach has been used to parameterize the main wing, nacelle, pylon, and horizontal and vertical tail surfaces. To treat the pod (the axisymmetric body atop the vertical tail) and aft fuselage surfaces, BANDAIDS[16] has been used. This technique is more appropriate for general surface topologies and provides a set of design variables describing general displacements normal to a surface. For simplicity, the intersections between aircraft components are held fixed, although this is not a requirement of the formulation. A total of 1384 design variables were used to parameterize the shaded regions of the surface mesh shown in Figure 11, but only 633 of them are active during the optimization.

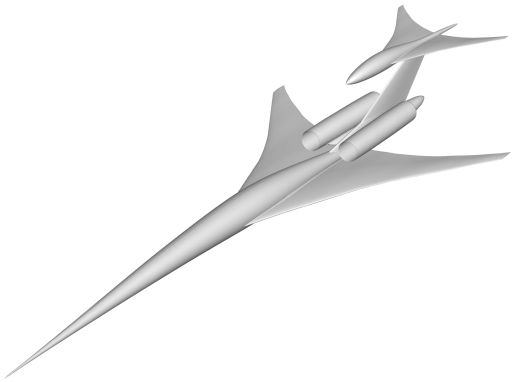

Figure 9. Overall view of the configuration

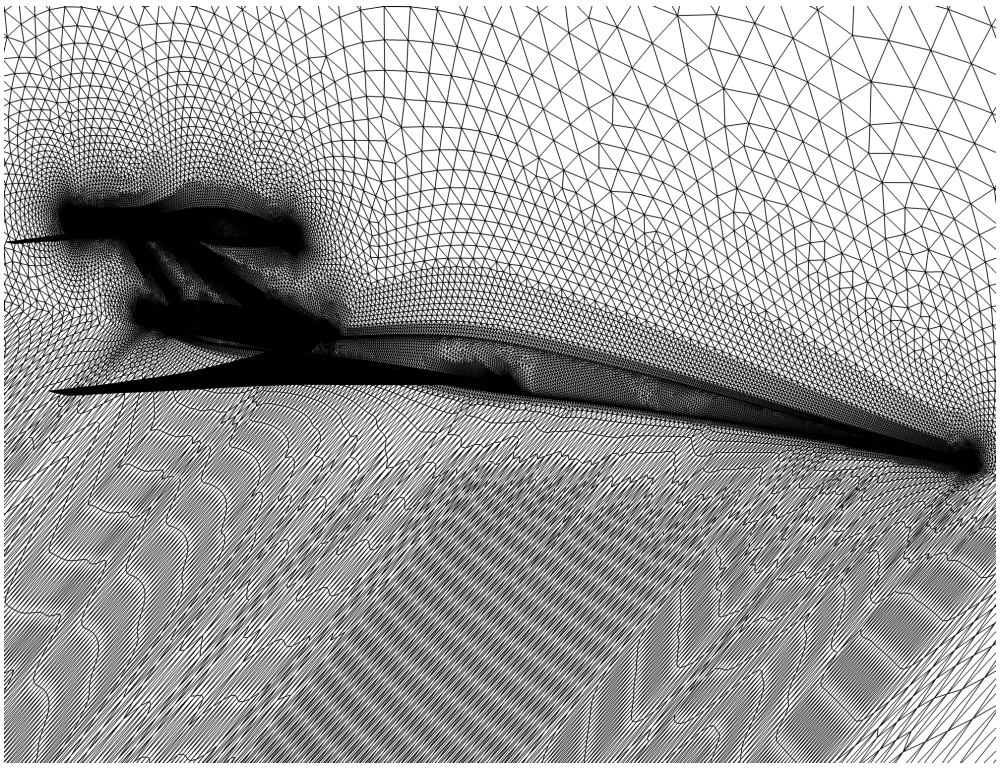

Figure 10. CFD grid

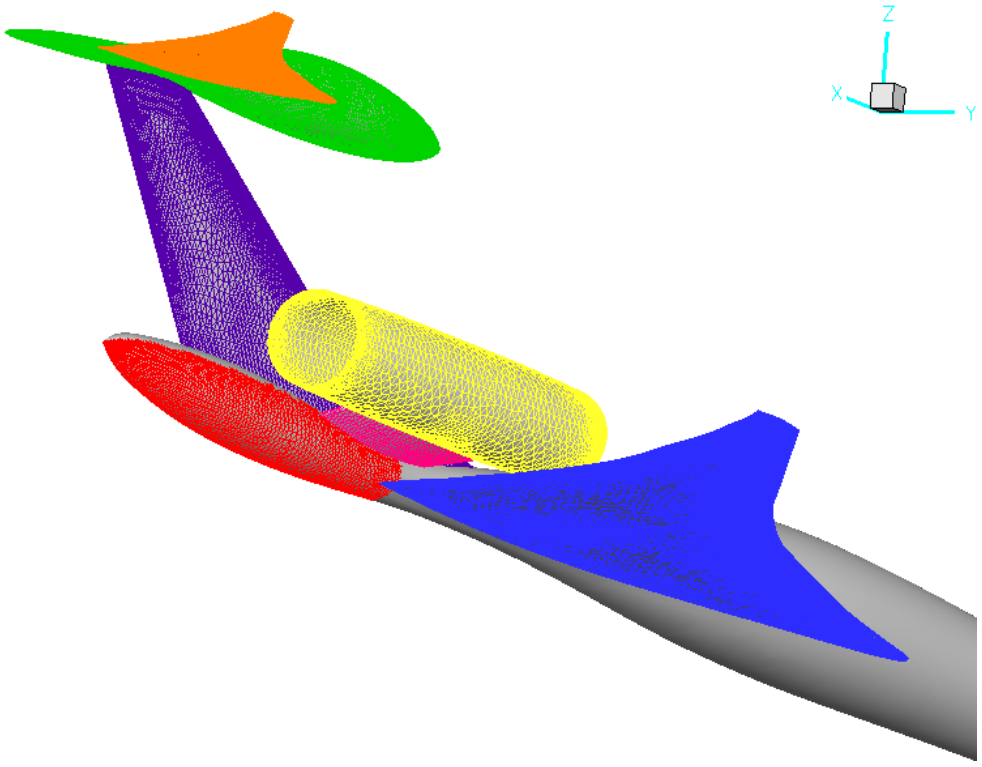

Figure 11. Parameterized components

Before the coupled CFD/boom implementation can be used for design, the adjoint derivatives need to be verified against complex sensitivities. For this purpose, FUN3D is run in forward-mode using small imaginary perturbations of arbitrary shape design variables and the resulting complex near-field signature is provided for propagation. The boom propagation process with complex input is then run to obtain the sensitivity of the cost function with respect to the perturbed design variable. This value is compared against that obtained using the coupled-adjoint implementation. A design variable perturbation and the corresponding FUN3D complex flow solution are depicted in Figures 12, 13 and 14. Figure 12 depicts the coutours of the sensitivity (dz/dD) of the vertical mesh deformation (z) with respect to a wing thickness design variable and the red colored contour region is the mesh that is affected by the perturbation in that particular wing thickness variable. Figure 13 plots the pressure contours, while Figure 14 is more interesting as it plots the sensitivity of the pressure field with respect to the wing thickness variable. This plot suggests that perturbation of the wing thickness as in Figure 12 has a much larger region of influence on the pressure field.

Table 2 shows the comparison of the sensitivities from both methods. It is seen that the values match well with each other; however the agreement is not accurate to machine precision. Due to the presence of a flux limiter, convergence to about 3 orders of magnitude short of machine precision is achieved. Flux limiting stalls convergence; the agreement between the sensitivities would be more exact if the limiter was not used and/or convergence of the solution to machine zero could be achieved.

Table 2. Comparison of the Coupled-Adjoint and Coupled-Complex Gradients

Shape Design Variable	Coupled-Adjoint Gradient	Coupled-Complex Gradient
Wing thickness	0.000016413373890	0.000016413359558
Nacelle thickness	0.000003136786602	0.000003136785870
Htail twist	0.000000528262959	0.000000528262256
Pylon camber	0.000000377252222	0.000000377250467
Vtail thickness	0.000002732768949	0.000002732764644
Fuselage bandaid	-0.000002310048595	-0.000002310050818
Pod bandaid	-0.000000257553786	-0.000000257553099

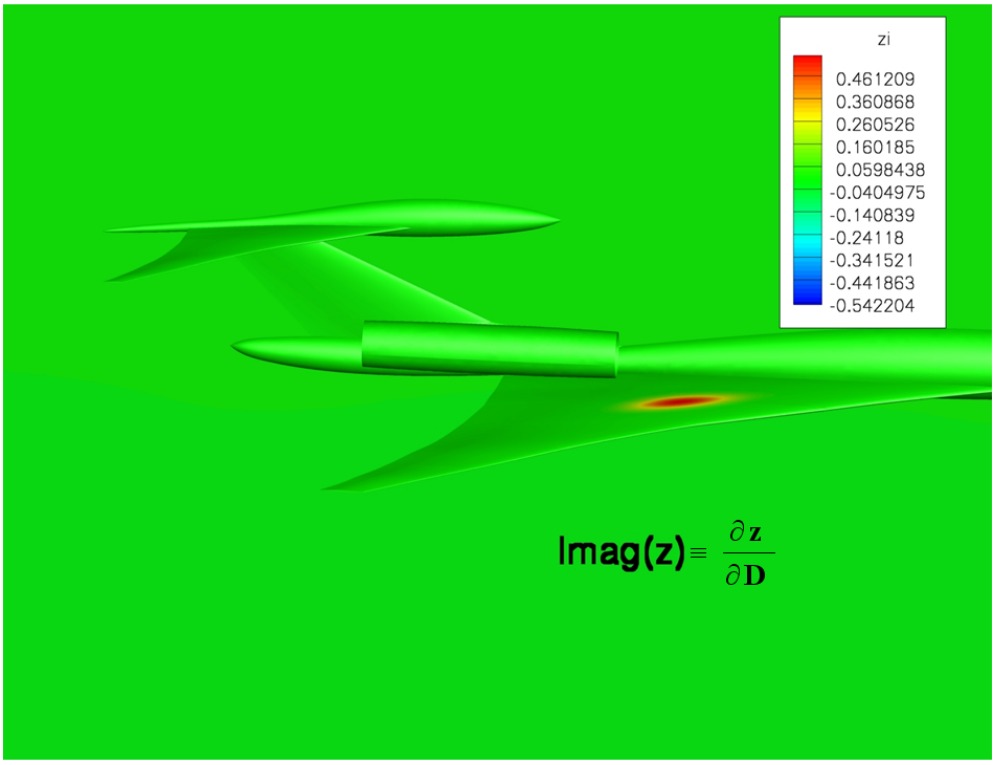

Figure 12. Mesh sensitivity to wing thickness perturbation

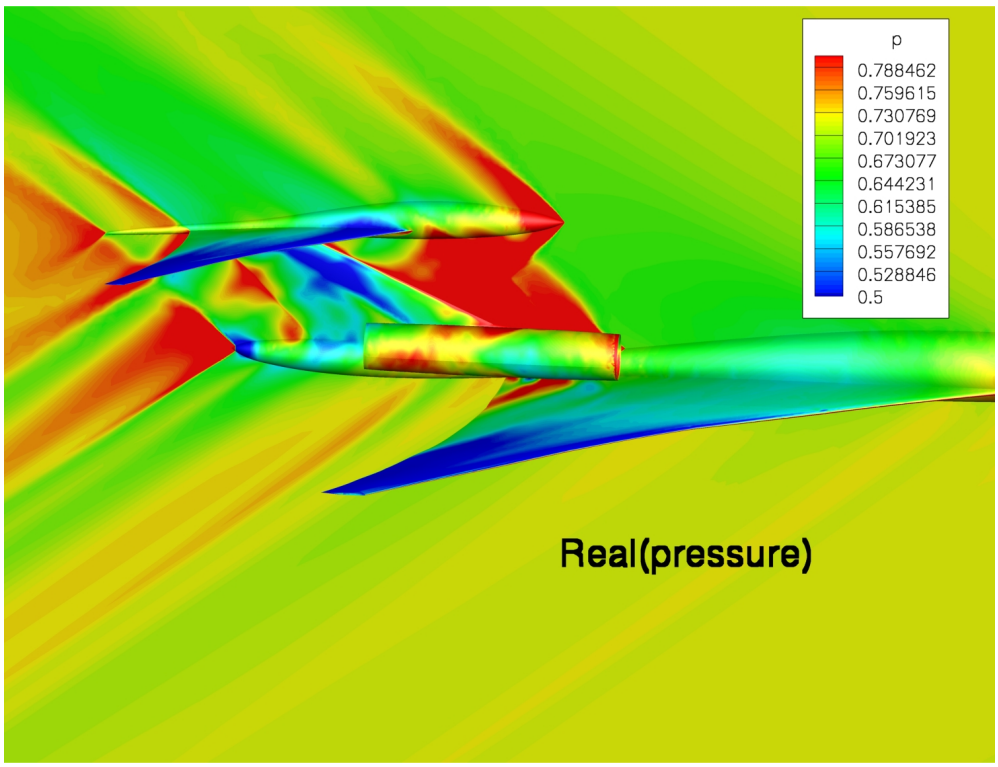

Figure 13. Flow-field pressure

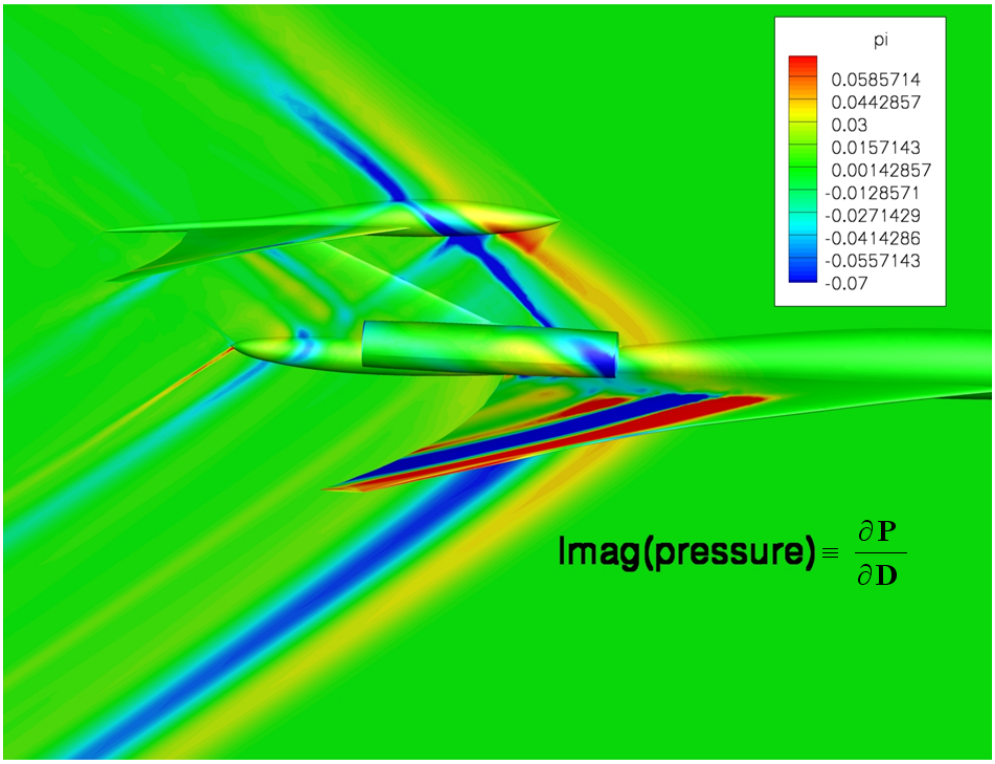

Figure 14. Flow-field pressure sensitivity

The same objective function as before is used to drive the design towards the design target. During optimization, the raw derivatives, such as those from Table 2, are scaled up by a factor of $1.e6$ to ensure that a unit change in the design variable causes approximately a unit change in the objective value. Optimization packages such as PORT[17] and NPSOL[18] that are already integrated with FUN3D were used for objective minimization. Figure 15 shows the baseline, target and the design ground signatures. It is seen that the design signature is closer to the desired target than the baseline; however the optimizer convergence is premature. The reasons for this could be manyfold with the primary ones being:

- The choice of design variables and their ranges are perhaps not sufficient to allow sufficient control of the geometry changes needed to reach the target ground signature
- The choice of the cost functional may be too restrictive.

The objective value history through several design iterations is depicted in Figure 16. After 5 iterations, the optimizer converges on a design that has a ground signature loudness of 80.4, which is approximately 3 dB lower than the baseline value of 83.5 on a perceived (PLdB) loudness scale.

An optimization of the coupled system such as that shown in Figure 16 requires 18 nearfield flow solutions and 8 nearfield adjoint solutions using FUN3D. For this study, 80 dual-socket nodes with Intel Xeon X5670 hex-core processors are used in a fully-dense fashion for a total of 960 computational cores. Each nearfield flow and adjoint execution uses 400 timesteps to converge the solution approximately 6 orders of magnitude, with each solution requiring roughly 1.5 minutes of wall-clock time. The additional components required for the optimization such as the forward and adjoint propagation process and the evaluation of the parameterized CFD surface meshes are serial applications and result in a total wall-clock time of approximately 1.5 hours for the optimization depicted in Figure 16, although the majority of the improvements are achieved in half that amount of time.

VI. Discussion

This study demonstrated that a sonic boom adjoint procedure could be used to obtain near-field pressure distributions that generate desirable ground signatures. This procedure allows the use of direct design techniques as opposed to the inverse design process generally used in supersonic aircraft design for sonic boom minimization. The integration of boom adjoint capability with CFD adjoint capability to obtain the sensitivity of any objective defined at the ground level with respect to the aircraft shape

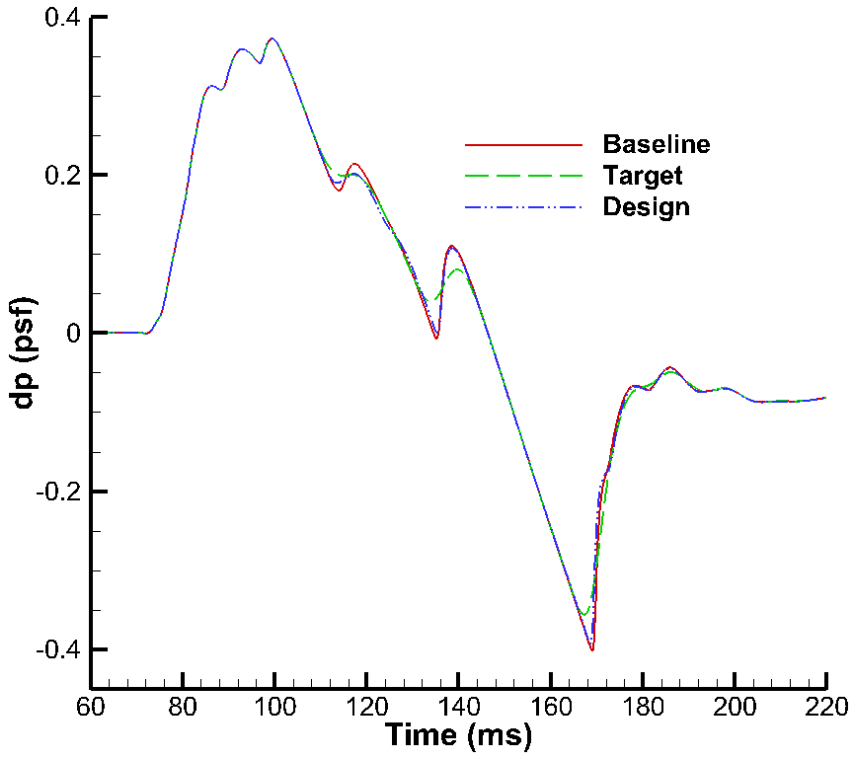

Figure 15. Ground signature comparison after CFD shape optimization

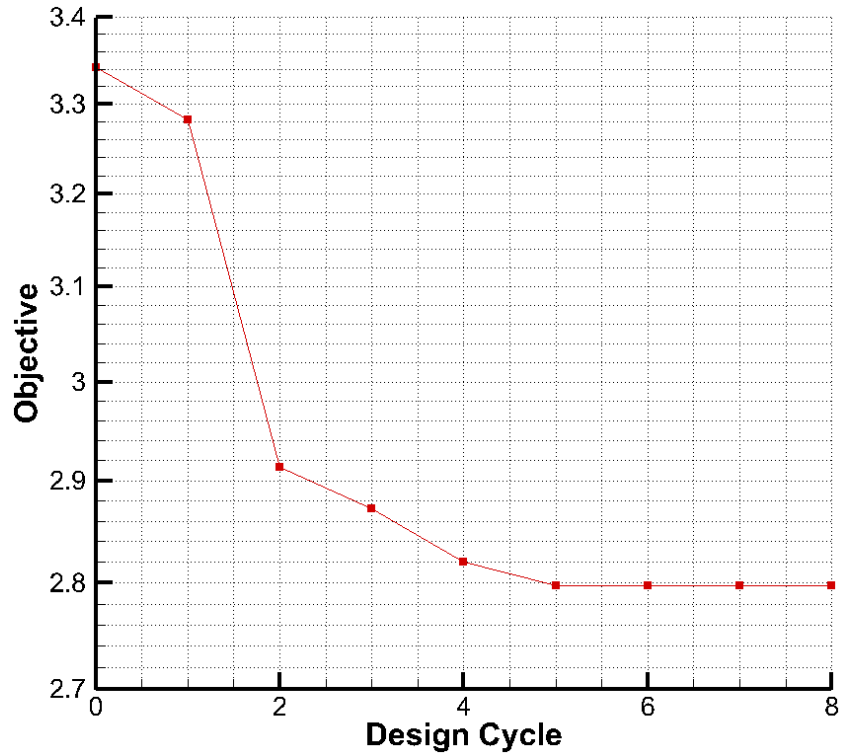

Figure 16. Convergence progress of CFD shape optimization

design variables could be an extremely useful tool because it formally couples CFD with ground signatures without the need for heuristics in the adaptation or design process. CFD codes such as FUN3D[2] and Cart3D,[19] which have adjoint capability, are ideally suited for this integration. Additional studies are required to identify effective design variables and to generate appropriate cost functionals. The crucial take-away is that we now have additional and potentially very powerful tools in our toolbox to attack the problem in several ways. This process can be refined and explored in better and efficient ways in the near future. Another dimension of research using this formulation stems from the acknowledgment that multiple near-field waveforms can lead to a single ground signature. This in turn leads to the argument that optimizers may achieve one of the several possible near-field waveforms which achieve the desired target, but have poor or sub-optimal off-design performance. An effective strategy to address this is a multi-point design to achieve robustness across different design and off-design conditions.

Using the adjoint sensitivities, the nature of localization of the shape changes needed to proceed towards desired ground signatures can be studied and understood. This also allows designers to analyze and study which shocks in the near-field signature correspond to the desired changes in the ground signature and provides a better perspective on the propagation process. The sensitivities of the sonic boom ground signature computed in this paper are with respect to the near-field pressure waveform. However, sensitivities can be obtained with respect to different design variables such as atmospheric parameters, or relaxation parameters, etc. This allows the designer to know how the choice of different propagation related parameters affect the ground signatures. Another interesting application is in the consideration of the off-design performance. If multiple ground signatures at design/off-design Mach numbers or under-/off-track azimuths each have their target ground signatures, then multiple adjoint solutions and their corresponding gradients can be used to simultaneously account for optimizing boom for design and off-design conditions. This could be extremely useful in multi-point, robust design studies.

VII. Conclusions

A sonic boom ground signature sensitivity method has been developed using the discrete adjoint approach and augmented Burgers' equation. The adjoint problem for the augmented Burgers' equation is derived, and the relevant sonic boom ground signature sensitivities are computed and verified. Integration of the boom adjoint method into a high-fidelity CFD and shape optimization environment for designing low-boom supersonic aircraft concepts has been described. The boom adjoint method and the formal adjoint-coupling between boom ground signatures and CFD presented in this study are not found in any existing literature. This study signifies a big step forward in the high-fidelity design capability and has immense potential for shape tailoring and optimization of supersonic aircraft. Future work will include refining and enhancing this capability as needed for improving low-boom supersonic aircraft concepts.

Appendix

The tridiagonal matrices for the relaxation processes are:

$$A^n, A_2^n = \begin{pmatrix} 1 & 0 & \cdots & & & \\ 0 & 1 & 0 & \cdots & & \\ 0 & -\alpha\kappa_1 - \kappa_2 & (1+2\alpha\kappa_1) & \kappa_2 - \alpha\kappa_1 & \cdots & \\ & \ddots & \ddots & \ddots & & \\ & & \cdots & 0 & 1 & 0 \\ & & \cdots & & 0 & 1 \end{pmatrix}$$

$$B^n, B_2^n = \begin{pmatrix} 1 & 0 & \cdots & & & \\ 0 & 1 & 0 & \cdots & & \\ \alpha'\kappa_1 - \kappa_2 & (1-2\alpha'\kappa_1) & \kappa_2 + \alpha'\kappa_1 & \cdots & & \\ & \ddots & \ddots & \ddots & & \\ & & \cdots & 0 & 1 & 0 \\ & & \cdots & & 0 & 1 \end{pmatrix}$$

In the above matrices, $\kappa_1 = \frac{C_\nu \Delta\sigma_n}{\Delta\tau^2}$, $\kappa_2 = \frac{\theta_\nu}{2\Delta\tau}$, and $\alpha' = 1 - \alpha$. If using the Crank-Nicholson scheme, $\alpha = 0.5$. For thermo-viscous absorption, the matrices are given below with $\lambda = \frac{\Delta\sigma_n}{2\Gamma(\Delta\tau)^2}$

$$A_3^n = \begin{pmatrix} 1 & 0 & \cdots & \\ -\lambda & (1+2\lambda) & -\lambda & \cdots \\ & \ddots & \ddots & \ddots \\ & & \cdots & 0 \quad 1 \end{pmatrix}$$

$$B_3^n = \begin{pmatrix} 1 & 0 & \cdots & \\ \lambda & (1-2\lambda) & \lambda & \cdots \\ & \ddots & \ddots & \ddots \\ & & \cdots & 0 \quad 1 \end{pmatrix}$$

Acknowledgments

This work was supported by the NASA Project entitled "Multi-fidelity Conceptual Design Process," under NASA contract number NNL08AA00B. Boris Diskin and Eric Nielsen were instrumental in the work concerning coupling and integration with FUN3D, and Bill Jones devoted time and effort into creating a geometry parameterization for CFD adjoint shape design and verification. All three contributed heavily to the sections related to CFD integration and the corresponding results and their contributions are much appreciated. Thanks are due to Dick Campbell for providing a stretched CFD grid. The author would like to thank Boris Diskin, and Mike Park for discussions related to the adjoint methodology; thanks are due to Irian Ordaz for some initial discussions. The support received from the entire supersonics airframe design tools team at NASA Langley Research Center is gratefully acknowledged.

References

[1]Pawlowski, J. W., Graham, D. H., et al., "Origins and Overview of the Shaped Sonic Boom Demonstration Program," AIAA Paper 2005-5, Jan. 2005.

[2]Nielsen, E. J. et al., "FUN3D: Fully Unstructured Navier-Stokes," http://fun3d.larc.nasa.gov/, accessed June 2011.

[3]Rallabhandi, S. K., "Advanced Sonic Boom Prediction Using Augmented Burger's Equation," AIAA Paper No. 2011-1278, Jan. 2011.

[4]Cleveland, R. O., "Propagation of Sonic Booms Through a Real, Stratified Atmosphere," Ph.D. thesis, University of Texas at Austin, 1995.

[5]Conte, S. D. and deBoor, C., *Elementary Numerical Analysis*, McGraw-Hill, New York, 1972.

[6]Nielsen, E. J., Diskin, B., and Yamaleev, N. K., "Discrete Adjoint-Based Design Optimization of Unsteady Turbulent Flows on Dynamic Unstructured Grids," *AIAA Journal*, Vol. 48, No. 6, 2010, pp. 1195–1206.

[7]Lyness, J. N., "Numerical Algorithms Based on the Theory of Complex Variables," *Proceedings of the ACM 22nd National Conference*, 1967, pp. 124–134.

[8]Lyness, J. N. and Moler, C. B., "Numerical Differentiation of Analytic Functions," *SIAM Journal on Numerical Analysis*, Vol. 4, 1967, pp. 202–210.

[9]Nielsen, E. J. and Jones, W. T., "Integrated Design of an Active Flow Control System Using a Time-Dependent Adjoint Method," *Mathematical Modeling of Natural Phenomena*, Vol. 6, No. 3, 2011, pp. 141–165.

[10]Park, M. A. and Darmofal, D. L., "Validation of an Output-Adaptive, Tetrahedral Cut-Cell Method for Sonic Boom Prediction," *AIAA Journal*, Vol. 48, No. 9, 2010, pp. 1928–1945.

[11]Park, M. A., "Low Boom Configuration Analysis with FUN3D Adjoint Simulation Framework," AIAA Paper No. 2011-xxxx, June 2011.

[12]Kleb, W. L., Nielsen, E. J., Gnoffo, P. A., Park, M. A., and Wood, W. A., "Collaborative Software Development in Support of Fast Adaptive Aerospace Tools (FAAST)," AIAA Paper No. 2003-3978, June 2003.

[13]Pirzadeh, S., "Three-Dimensional Unstructured Viscous Grids by the Advancing-Layers Method," *AIAA Journal*, Vol. 34, No. 1, 1996, pp. 43–49.

[14]Campbell, R. L., Carter, M. B., Deere, K. A., and Waithe, K. A., "Efficient Unstructured Grid Adaptation Methods for Sonic Boom Prediction," AIAA Paper 2008-7327, Aug. 2008.

[15]Samareh, J. A., "A novel shape parameterization approach," Tech. Rep. NASA TM-1999-209116, NASA Langley Research Center, Hampton, VA, May 1999.

[16]Samareh, J. A., "Aerodynamic Shape Optimization based on free-form deformation," AIAA Paper No. 2004-4630, 2004.

[17]Blue, J., Fox, P., Fullerton, W., et al., "PORT Mathematical Subroutine Library," http://www.bell-labs.com/project/PORT/, accessed June 2011.

[18]Gill, P. E., Murray, W., et al., "NPSOL: A Fortran Package for Nonlinear Programming," http://www.sbsi-sol-optimize.com/, accessed June 2011.

[19]Nemec, M. and Aftosmis, M., "Parallel Adjoint Framework for Aerodynamic Shape Optimization of Component-Based Geometry," AIAA Paper No. 2011-1249, Jan. 2011.